THE EUROPEAN
PHYSICAL JOURNAL
SPECIAL TOPICS

Regular Article

Mid-range natural orbits around the triple asteroid 2001SN$_{263}$

M.P.O. Cavalca[1], V.M. Gomes[2], and D.M. Sanchez[1,a]

[1] National Institute for Space Research – INPE, São José dos Campos, São Paulo 12227-010, Brazil
[2] São Paulo State University – UNESP/FEG, Guaratinguetá, São Paulo 12516-410, Brazil

Abstract. The goal of the present paper is to search for natural trajectories that can be used to place a spacecraft to observe the triple asteroid 2001SN$_{263}$. For a first set of observations mid-range distance orbits are ideal. To model this triple asteroid from a mid-range distance, it is considered that it can be modeled as a single ellipsoid body, which gives a simple mathematical model that allows on-board computation of trajectories. The mass is assumed to be equal to the sum of the masses of the three bodies and its dimensions are calculated considering the size of the orbits of Beta and Alpha. The objective is to search for orbits that can be used at the arrival time of the spacecraft in the vicinity of the triple asteroid to observe the bodies to make a better evaluation of their dimensions and dynamics before a good choice for a final orbit can be made. The two-dimensional elliptic restricted three-body problem is used as the mathematical model with the addition of the perturbations coming from the asteroid and the Sun irregular gravity fields (J_2). It is also considered the disturbance caused by the solar radiation pressure, a major force near asteroids.

1 Introduction

In recent years the number of missions and studies to small bodies such as dwarf planet, comets, and asteroids has increased [1]. In addition to the problem that many of these bodies are located thousands of miles away, they may still present very curious shapes [2], that can also be composed by two or more bodies [3], and may also present rings [4,5]. For all these different characteristics it is very challenge to idealize a physical and dynamical model for these bodies, as well as strategies that allow mission operations in a safe and efficient way without risks of collisions or escapes of the space vehicle from the system.

Some techniques that make possible to model the shape of small bodies are already known. The polyhedron method consists in modeling the shape of the body in a certain number of polyhedrons connected by faces but it needs a close and accurate analysis of the body [6]. The dipole and tripole methods are simplified models compared to the previous one but are useful in analyzing the dynamics of the system

---

[a] e-mail: diogo.sanchez@inpe.br

with respect to the particular characteristics of the bodies [7]. However, these methods must be applied after a detailed study of the body or bodies and are generally used when the spacecraft is very close to its target in the phase of controlled impact or landing. The arrival of the Rosetta mission proposed by ESA [8], when close to its target, the comet 67P/Churyumov-Gerasimenko, is a recent example of how important is to propose new techniques for approaching distant bodies. After 10 years of travel and only 4 months after sending the module Philae to the surface to the comet, it was observed that the shape of the asteroid did not resemble the model assumed during the initial mission studies [9].

The purpose of this paper is to perform a numerical search for trajectories close to the vicinity of the Near-Earth Asteroid (NEA) 2001SN$_{263}$ [10–12], classified as Amor-type NEA, which means that its perihelion distance is between 1.017 au and 1.3 au, where 1 au is one astronomical unit. This asteroid is a triple system. The largest body of the system, Alpha, has a mass equal to 917.466×10^{10} kg, and a radius equal to 1.3 km. Beta is the second largest body of this system, located at 16.633 km from Alpha, with a mass equal to 24.039×10^{10} kg and a radius equal to 0.39 km. Beta is also near a planar orbit with respect to the longitudinal axis of Alpha. Gamma is the smallest body, with mass and radius equal to 9.773×10^{10} kg and 0.29 km, respectively. It is located at 3.804 km from Alpha with an inclination of 13.87 degrees with respect to the longitudinal axis of Alpha. Both Beta and Gamma have almost circular orbits around Alpha. The orbit of the system is highly eccentric, with an eccentricity of 0.48 and semi-major axis equal to 1.99 au with respect to the Sun. The main reason to study this asteroid is that it is the goal of a proposed mission [13] that plans to use a low thrust [14–17] to send a spacecraft to the Moon to make a powered Swing-By [18] to direct the spacecraft to this asteroid. For this study the triple asteroid will be considered as a single elongated body with triaxial symmetry [19]. Its longitudinal radius is equal to 16.633 km, which is the distance between Alpha and Beta and its height is equal to 1.3 km, which is the radius of Alpha. Its mass is considered equal to 951.278×10^{10} kg, which is the sum of the masses of the three bodies. Figure 1 shows this situation. The goal is to search for trajectories in the vicinity of the triple asteroid, but far enough to consider it as a single elongated asteroid. There are still many inaccuracies in the masses, sizes, and distances of bodies of this type, so the idea of analyzing the system from a large safe distance, to obtain more precise measurements, is important. After that we can really approach the asteroid. The system that will be considered is composed by the Sun, the elongated asteroid and the space vehicle. The motion of the space vehicle in the vicinity of the asteroid will be described by the elliptic restricted three-body problem [20], added by the influence of the term J_2 due to the equatorial flattening of the Sun and the elongated asteroid [21], The influence of the solar radiation pressure (SRP) [22] will also be considered in the dynamical model. The solar radiation pressure will be considered using different values of the ratio area-to-mass (A/m) of the spacecraft. A study will also be carried out on the effect of perturbations in the motion of the space vehicle due to the gravitational interaction and the term J_2 of the bodies and the solar radiation pressure. This study will be done for different integration times and using the perturbation integral [23,24]. Finally, the results show different patterns of trajectories in the neighborhood of the elongated asteroid that can be used according to the objective of this phase of the mission, as for example, to orbit a specific region of the asteroid, to escape from its influence or to get closer to it. The trajectories are identified by each set of initial conditions, which are the position and velocity of the spacecraft relative to the elongated asteroid. In order to select the trajectories, we use the values of the minimum, maximum and average distances between the spacecraft and the elongated asteroid, which are shown in color maps [25,26].
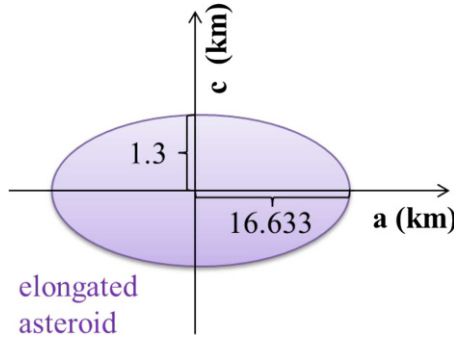
Fig. 1. Dimensional model of the elongated asteroid.

2 Mathematical and dynamical model

In this section the mathematical model of the dynamics is presented. The system is formed by the Sun, the elongated asteroid and the spacecraft. Equation (1) is the equation of motion of the space vehicle. The first two terms refer to the influence of the gravitational forces of the Sun and the elongated asteroid, using the elliptic restricted three-body problem. The term ($\mathbf{P}_{J2}$) refers to the influence of the terms J_2 due to the flattening of the Sun and the elongated asteroid. The last term refers to the influence of the solar radiation pressure ($\mathbf{P}_{\text{SRP}}$), which has direct dependence on the area/mass ratio of the spacecraft.

$$\ddot{\mathbf{r}} = G\left(-m_1 \frac{\mathbf{r_1}}{\mathbf{r_1}^3} - -m_2 \frac{\mathbf{r_2}}{\mathbf{r_2}^3}\right) + \mathbf{P}_{J2} + \mathbf{P}_{\text{SRP}}. \tag{1}$$

In equation (1), G represents the gravitational constant, m_1 and m_2 refer to the Sun and the elongated asteroid masses, respectively. The distances r_1 and r_2 correspond to the distance Sun-spacecraft and elongated asteroid-spacecraft, respectively. Equation (2) shows the accelerations given by the effect of the term J_2 of the flattening of the Sun and of the elongated asteroid:

$$\mathbf{P}_{J2} = -m_1 J_2^{M1} R_{M1}^2 \left(\frac{3(x+y)}{2\mathbf{r}_1^5}\right) - m_2 J_2^{M2} R_{M2}^2 \left(\frac{3(x+y)}{2\mathbf{r}_2^5}\right) \tag{2}$$

where the J_2 term for the elongated asteroid is given by equation (3) [19]:

$$J_2^{M2} = \frac{(a^2 - c^2)}{5R_{M2}^2} \tag{3}$$

where the average longitudinal radius of the elongated asteroid is given by R_{M2}, a is equal to R_{M2} and c is the transversal radius. The influence of the solar radiation pressure is given by equation (4).

$$\mathbf{P}_{\text{SRP}} = -C_R P_S \frac{A}{m} \frac{\mathbf{r_S}}{|\mathbf{r_S}|^3} \tag{4}$$

where the reflectivity coefficient of the surface of the space vehicle is indicated by C_R, which is equal to 1 to represent a situation where there is total light absorption; the solar flux is indicated by P_S; the ratio of the cross-sectional area of the spacecraft to its mass is indicated by A/m. The distance between the Sun and the elongated asteroid is indicated by r_S and it is equal 1.99 au.

Table 1. Physical and orbital data of the Sun and elongated asteroid [27,28].

Celestial body	Average radius (km)	Mass (kg)	J_2	Semi-major axis (au)	Eccentricity
Sun	697500	$19\,885 \times 10^{30}$	22×10^{-7}	–	–
Elongated asteroid	16633	$951278 \times 10^{10}*$	0.198778*	199	048

*Calculated values.

Table 1 shows the physical and orbital data of the Sun [27] and the elongated asteroid. The physical data of the elongated asteroid were calculated according to the values of the triple asteroid $2001SN_{263}$ [28] where: the longitudinal radius is equal to the Alpha-Beta distance (16.633 km); the height is equal to the radius of Alpha (1.3 km); the mass is equal to the sum of the masses of Alpha, Gamma, and Beta (951.278×10^{10} kg); the flattening term J_2 is given by equation (2) (0.198778); the semi-axis (1.99 au) and the eccentricity (0.48) are measured relative to the Sun.

Figure 2 shows the initial geometry of the problem in which the Sun, the elongated asteroid and the space vehicle are aligned in the x-axis of the fixed reference system. The spacecraft is at an initial distance D from the asteroid and has initial velocity with components v_x and v_y. These three parameters are the initial conditions of the spacecraft relative to the asteroid. Initially, a search is made in which the three parameters are changed, and the respective trajectories are integrated in time. The maximum (D_{max}), minimum (D_{min}), and average (D_{avg}) distances of spacecraft-asteroid are calculated and can be used as a criterion to select the orbits [26,27]. One of the objectives is to find initial conditions that generate trajectories that respect the following restrictions: Maximum and average distances less than 180 km ($D_{max} < 180$ km and $D_{avg} < 180$ km) and minimum distances greater than 50 km ($D_{min} > 50$ km). The reason is to find orbits that do not get too close to the asteroid, but also that do not go too far. These limits give trajectories close enough to observe the asteroid system but are still compatible with the model given by a single elongated body. After that, the values of the distances are sorted from the lowest to the maximum distances and then one of the initial conditions (D, v_x, or v_y) is selected to remain fixed, while the other two are varied within a range of values to build the color maps. The idea is to find the ranges of initial conditions that generate families of trajectories and not only isolated trajectories. Finally, the trajectory is drawn by choosing a specific set of initial conditions. Another objective is to study the influence of the solar radiation pressure in the trajectories of the spacecraft by varying the A/m ratio. Three values of A/m used in this study are: zero, 0.001, and 0.01 m^2/kg, which means that three cases are analyzed: without considering the solar radiation pressure ($A/m = 0$), considering the solar radiation pressure in a spacecraft that has the dimensions of a standard spacecraft ($A/m = 0.001$ m^2/kg), and considering that the spacecraft has a sail or a solar panel ($A/m = 0.01$ m^2/kg).

The criterion to select orbits is based on calculating, for each set of initial conditions, the maximum (D_{max}), minimum (D_{min}), and average (D_{avg}) distances between the spacecraft and the elongated asteroid during the entire integration time. Then those distances are classified according to what is desired for the mission. The average distance is obtained from equation (5) shown next:

$$D_{avg} = \frac{1}{T} \int_0^T r_2\,(t)\,dt \tag{5}$$

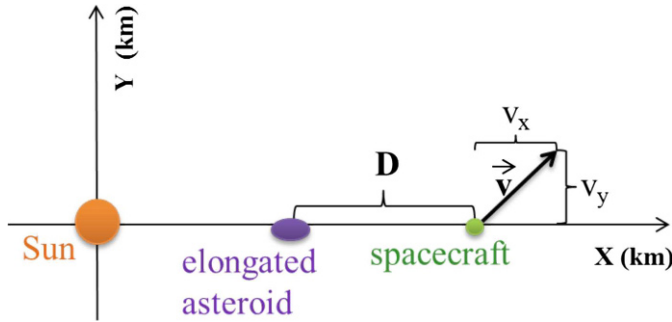where the total integration time is given by T.

Fig. 2. Schematic drawing of the problem in the fixed reference system.

Next it is explained the Integral Perturbation Method, which is used to calculate individually how much a force acts in the motion of the vehicle. Among several options for this type of study [29,30] it is chosen the integral of the magnitude of the force, because the goal is to compare the forces. It means that the index is defined by equation (6) shown below:

$$PI = \frac{1}{T} \int_0^T |\boldsymbol{\alpha}| \, dt \qquad (6)$$

where T is the total integration time and α is the acceleration vector given by the force considered. In this study, the forces considered are the ones due to the gravitational interaction of the Sun (PertSun) and the elongated asteroid (PertAster); the terms J_2 representing the flattening of the Sun (PertJ2Sun) and the elongated asteroid (PertJ2Aster); and the solar radiation pressure (PertSRP). There are three more types of integral indices that can be used for other cases and that can be seen in more detail in [31].

3 Analysis and results

After identifying trajectories of interest, specified by the position and velocity of the spacecraft relative to the asteroid, new integrations are made using smaller spacing in the parameters. After that, color maps are generated to show the trajectories in more detail.

3.1 Study considering $A/m = 0$

Figure 3 shows the color maps for the case where the solar radiation pressure was not considered in the model ($A/m = 0$) and the integration time is equal to 90 days. From there we can observe and analyze the distribution of distances and the effects of the forces as a function of the initial conditions of a space vehicle in the neighborhoods of an elongated asteroid. The values of the initial distance D range from 50 to 70 km; the velocity v_y range from -0.00015 to 0.00015 km/s; and the velocity v_x remains fixed at zero. The distributions of maximum, minimum, and mean distances are shown in Figures 3a–3c, respectively. The effects of the forces due to the interaction with the asteroid, the J_2 terms of the asteroid and the Sun are shown in Figures 3d–3f, respectively. The blank regions in Figures 3a–3c indicate initial conditions that do not respect the restrictions $D_{max} < 180$ km, $D_{avg} < 180$ km, and $D_{min} > 50$ km.
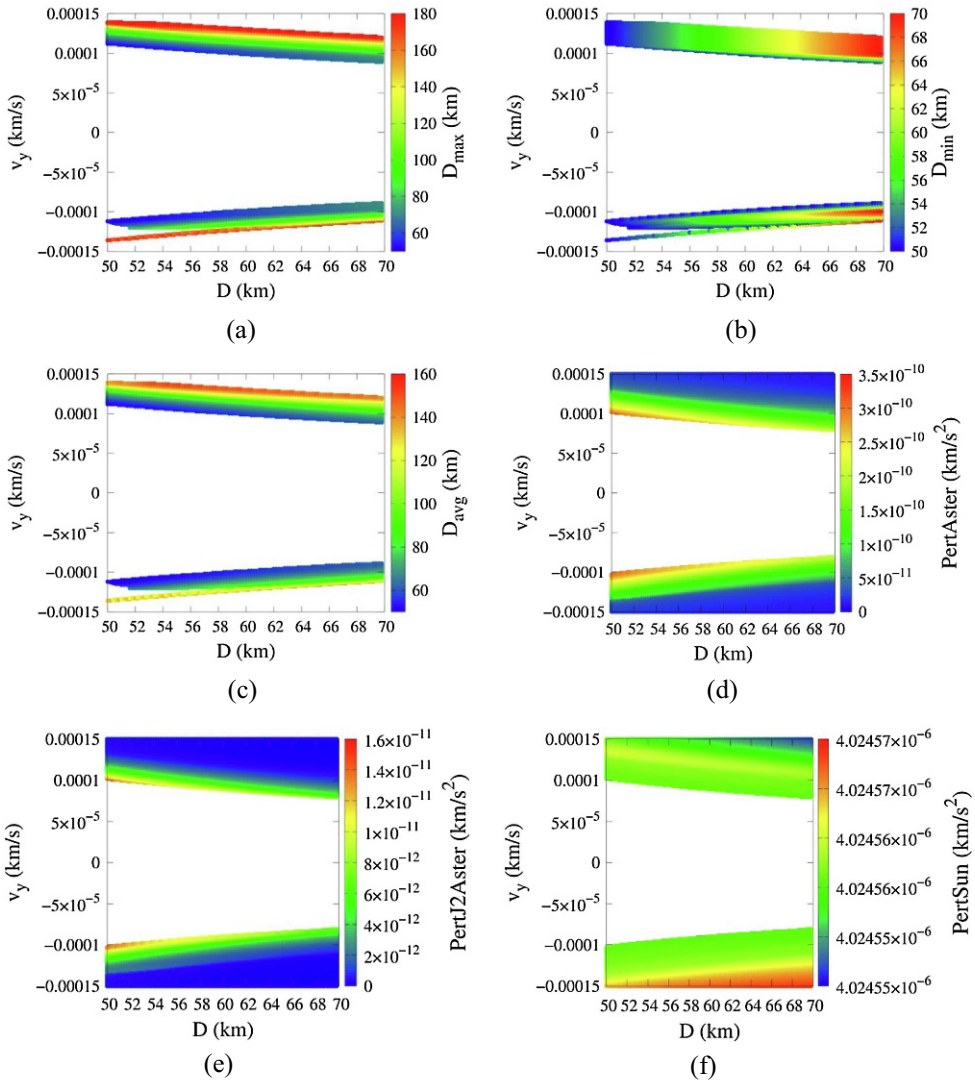
Fig. 3. Color mappings for $A/m = 0$ and $T = 90$ days for the variation of (a) D_{max}, (b) D_{min}, (c) D_{avg}, (d) PertAster, (e) PertJ2Aster, and (f) PertSun.

Among them there are the initial conditions that lead the spacecraft to collide with the elongated asteroid. In the case of Figures 3d–3f, only the initial conditions that cause the spacecraft to collide with the elongated asteroid are blank. The figures showing the contribution of each force are not limited by the distance constraints and all the solutions are shown. The values with respect to the force due to the J_2 term of the Sun were all equal to 2.21×10^{-17} km/s^2.

It is also possible to identify, from Figure 3, which set of initial conditions generate the lower and the higher values of distances and also those that are more or the less affected by each force. The figures show certain symmetry in the dispersions of the values with respect to the y axis having the zero value as reference for the symmetry. However, in the figures of distances, Figures 3a–3c, it is noticed that the range of negative values of y presents a certain discontinuity for the values of
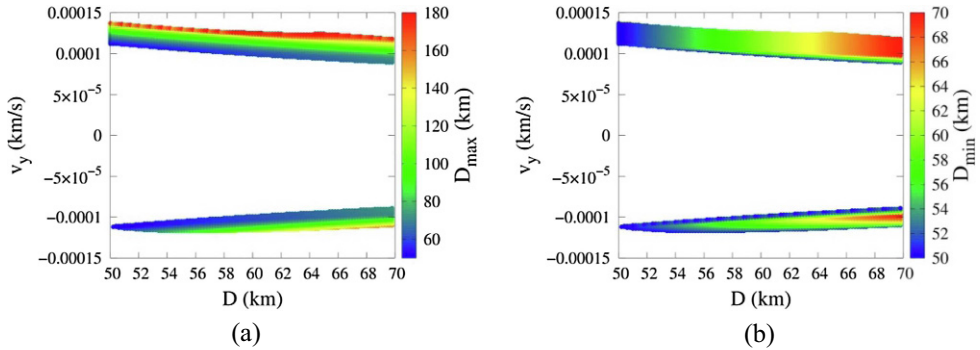
Fig. 4. Colors maps for $A/m = 0\,\mathrm{m}^2/\mathrm{kg}$: (a) $D_{\max}$ (b) $D_{\min}$ for $T = 240$ days.

x from 50 to 57 km. In the figures of maximum and average distances, Figures 3a and 3b, the highest values of distances are on the outer edges of the positive and negative bands of y, and the lower values are in the internal parts of these bands. The distribution of the minimum distances, shown in Figure 3b, presents the smallest values in the inner parts of the positive and negative y ranges. It is also observed that the minimum distances are distributed from the lowest to the highest values according to the values of D (km), the initial distance. It means that, as D increases, the minimum distance also increases. In the plots showing the effects of each force, Figures 3d–3f, the dispersion of the values is practically symmetrical with respect to zero on the y-axis. Remembering that these figures do not include the restrictions of maximum ($D_{\max} < 180\,\mathrm{km}$), minimum ($D_{\min} > 50\,\mathrm{km}$) and average ($D_{\mathrm{avg}} < 180\,\mathrm{km}$) distances. The perturbations related to the elongated asteroid, Figures 3d and 3e, behave inversely to those of maximum and average distances, Figures 3a and 3c, that is, the initial conditions that give more disturbances are in the inner part of the ranges of positive and negative y, and the less disturbed ones are in the outer parts of those bands. It is also observed that the lower values of D have larger perturbations, since these conditions are closer to the asteroid. The distribution of the effects of the Sun, Figure 3f, is practically equal to $4.0245 \times 10^{-6}\,\mathrm{km/s}^2$ and this is of course the dominating force acting along the trajectories.

After that, Figure 4 shows the color mappings of maximum ($D_{\max}$) and minimum ($D_{\min}$) distances as a function of the initial distance D, which varies from 50 to 70 km and the velocity v_{y} in the range -0.00015 to $0.00015\,\mathrm{km/s}$, with the velocity v_{x} being fixed in zero, similar to the values used in Figure 3, but now the study is extended to 240 days.

Observing Figure 4, it can be seen that, over the time, the initial conditions that generate the trajectories with higher values of $D_{\max}$ are the ones suffering the largest variations. It is also observed that the trajectories with smaller values of D are also the ones that suffer the most changes, because they stay longer closer to the asteroid. This occurs because, over the time, the trajectories can approach or move away from the elongated asteroid, not respecting the limits of the distances $D_{\max} < 180\,\mathrm{km}$ and $D_{\min} > 50\,\mathrm{km}$. Figure 5 presents two examples of trajectories, with the two sets of initial conditions taken from Figure 4. Set 1 considers: $D = 60\,\mathrm{km}$, $v_{\mathrm{x}} = 0$, and $v_y = 0.0001\,\mathrm{km/s}$; while set 2 considers $D = 60\,\mathrm{km}$, $v_x = 0$, and $v_y = -0.0001\,\mathrm{km/s}$. Figures 5a and 5b show the trajectory for set 1 considering the times of 90 and 240 days, respectively. Figures 5c and 5d show the trajectory for set 2, also considering the times 90 and 240 days, respectively. The rotating reference system is used and the elongated asteroid is represented in scale at the origin of the system.
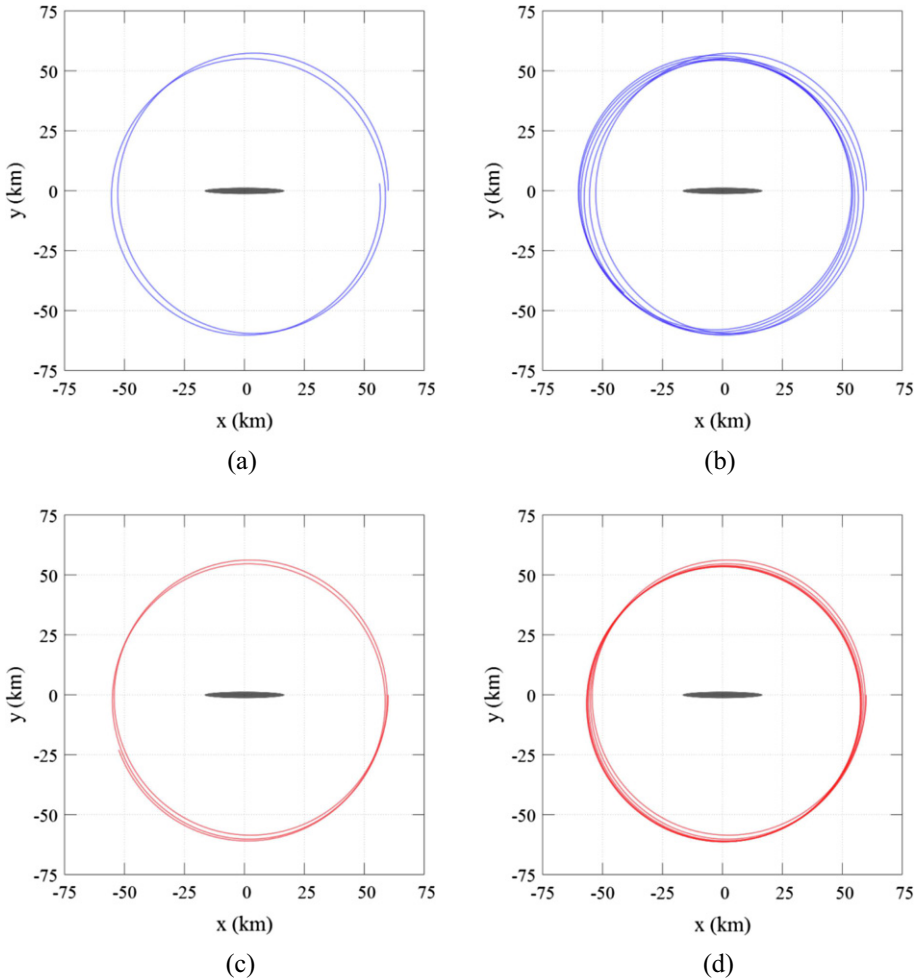
Fig. 5. Trajectories for $A/m = 0$ and simulations times of 90 and 240 days for two sets of initial conditions: (a) and (b) is for set 1; (d) and (e) is for set 2.

In Figure 5 the two trajectories can be observed around the elongated asteroid over the time. Set 1, shown in Figures 5a and 5b, were made using the positive values of v_y shown in Figure 4; while set 2 is made for the negative values of v_y shown in Figure 4. In set 1, the trajectories have the counterclockwise sense and v_y is equal to 0.0001 km/s. In set 2, the trajectories have clockwise sense and v_y is equal to -0.0001 km/s. It is observed that, for both sets 1 and 2, the trajectories present small oscillations, and set 1 presented larger visual variations over time. Table 2 shows the respective values of distances: maximum, minimum, and average; as well as the effects of the gravitational forces and the J_2 terms of the Sun and the elongated asteroid for each trajectory.

In Table 2 it is observed that the values of maximum and minimum distances for the set 1 for the times of 90 and 240 days were equal, and their values were 60.6011 and 52.7889 km, respectively. It is observed that the maximum and minimum distances of the set 1 are smaller than those presented by set 2, which are equal to 61.1504 and 54.0593 km, respectively, for the time of 90 days and 61.2685 and 53.4817 km, respectively, for the time of 240 days. In this condition, set 1 presents the largest

Table 2. Values of distances and perturbations for the trajectories with $A/m = 0$ considering set 1 and set 2.

	Set 1		Set 2	
	90 days	240 days	90 days	240 days
$D_{\max}$ (km)	60.6011	60.6011	61.1504	61.2685
$D_{\min}$ (km)	52.7889	52.7889	54.0593	53.4817
D_{avg} (km)	57.4337	57.2146	57.8400	57.5739
PertAster (km/s^2)	1.74×10^{-10}	1.75×10^{-10}	1.72×10^{-10}	1.74×10^{-10}
PertSun (km/s^2)	4.02×10^{-6}	2.48×10^{-6}	4.02×10^{-6}	2.48×10^{-6}
PertJ2Aster (km/s^2)	4.41×10^{-12}	4.47×10^{-12}	4.29×10^{-12}	4.38×10^{-12}
PertJ2Sun (km/s^2)	2.21×10^{-17}	1.03×10^{-17}	2.21×10^{-17}	1.03×10^{-17}

variation. Set 1 also presented the lowest average distances for the 90 and 240 days, 57.4337 and 57.2146 km, respectively. By analyzing the effects of the forces acting in the dynamics, it is observed that the Sun (PertSun) is the dominant force in the trajectories, as expected, being of the order of 10^{-6}, followed by the perturbation of the elongated asteroid (PertAster), which is of the order of 10^{-10}.

Next, the study of the distribution of the initial conditions is presented as a function of the A/m ratio and time. Three values of A/m are adopted: zero, when the solar radiation pressure is not considered; 0.001 and 0.01 m^2/kg, cases in which the solar radiation pressure is considered, but in different levels. Integration times are adopted according to the A/m value. Only the distribution charts of the maximum and minimum distances will be presented, since they are those that presented significant changes according to the case. The results for the average distances follow very closely the distribution of the maximum distances, because the minimum values are small. We will also present examples of trajectories over time for different sets of initial conditions, as well as their respective values of distances and effects of the forces.

3.2 Study considering $A/m = 0.001$ m^2/kg

In this second case the solar radiation pressure is considered, assuming a typical value for a spacecraft of $A/m = 0.001$ m^2/kg. Figure 6 shows the color maps of maximum ($D_{\max}$) and minimum ($D_{\min}$) distances as a function of the initial distance D, which varies from 50 to 70 km and the velocity v_{y}, which is in the range from -0.00015 to 0.00015 km/s, with the velocity v_{x} being fixed in zero. Figures 6a and 6b consider the time of 90 days and Figures 6c and 6d the time of 180 days.

In Figure 6 the same set of initial conditions used in the previous case, $A/m = 0$, is used to construct the color maps. In the present case, it is observed that the initial conditions that generate trajectories and have positive v_{y}, Figures 6a and 6b, are not present in Figures 6c and 6d. It means that these initial conditions, when considered for longer times, no longer respect any of the maximum or minimum distance restrictions. Through the distribution of minimum distances, shown in Figure 6b, it is observed that these conditions probably no longer respected the restriction $D_{\min} > 50$ km, because, for the time of 90 days, $D_{\min}$ is already close to this limit. Comparing Figures 6a and 6c we also note that the smaller starting distance values of D and the ones with the higher maximum distances for the 90 days period do not appear in the figures made using 180 days of simulation. Again, these initial conditions should no longer respect the constraints if we analyze Figures 6b and 6d. Compared to the simulations made for $A/m = 0.0$, it is clear the reduction of the sizes
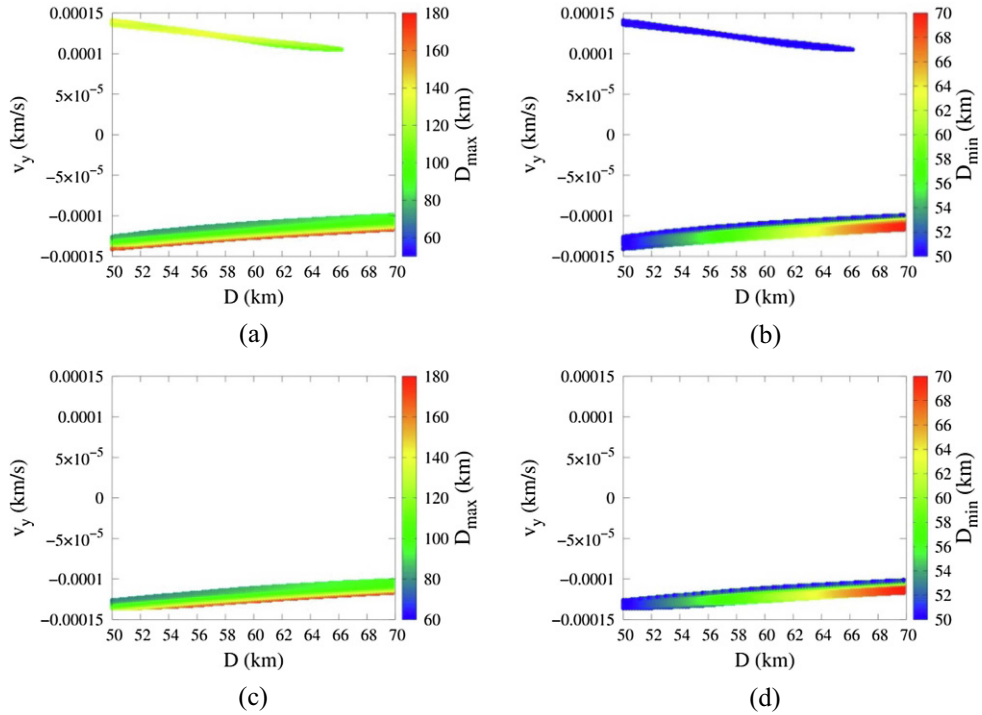
Fig. 6. Color maps for $A/m = 0.001\,\mathrm{m}^2/\mathrm{kg}$: (a) $D_{\max}$, (b) $D_{\min}$ for $T = 90$ days and (c) $D_{\max}$, (d) $D_{\min}$ for $T = 180$ days.

of areas generating trajectories that respect the distances constraints, which means that the solar radiation pressure reduces the number of acceptable trajectories.

Figure 7 shows two examples of trajectories, with the two sets of initial conditions taken from Figure 6. Set 1 considers: $D = 55\,\mathrm{km}$, $v_x = 0$, and $v_y = 0.000126\,\mathrm{km/s}$; and set 2 considers $D = 60\,\mathrm{km}$, $v_x = 0$, and $v_y = -0.00011\,\mathrm{km/s}$. Figures 7a and 7b show trajectories for set 1 considering the times of 90 and 120 days for the simulation, respectively. Figures 7c and 7d show trajectories for set 2 considering the times 90 and 180 days for the simulation, respectively. The idea is to show a trajectory that does not "survive" up to 180 days, given by set 1, and a trajectory that "survives" up to 180 days, given by set 2. The rotating reference system is used and the elongated asteroid is represented in scale at the origin of the reference system. It is observed that set 1 has a trajectory that starts at $D = 55\,\mathrm{km}$ and travels counterclockwise, moving around the elongated asteroid while it moves away from it, as seen in Figure 7a. However, Figure 7b shows that the trajectory tends to return and to move towards the elongated asteroid, which may indicate that, before the time of 180 days, it fails with respect to the limit $D_{\min} > 50\,\mathrm{km}$. Set 2, shown in Figures 7c and 7d, presents a trajectory that performs small oscillations, but that surrounds the elongated asteroid for up to the time of 180 days.

Table 3 shows the respective values of distances: maximum, minimum, and average; and the effects of the forces due to the Keplerian terms of the gravitational fields and the J_2 terms due to the flattening of the Sun and the elongated asteroid, for each trajectory.

In Table 3 it is observed that the values of maximum, minimum, and averages distances for the set 2, considering simulation times of 90 and 180 days, were equal and their values were 79.1862, 52.1923, and 66.8559 km, respectively. The highest
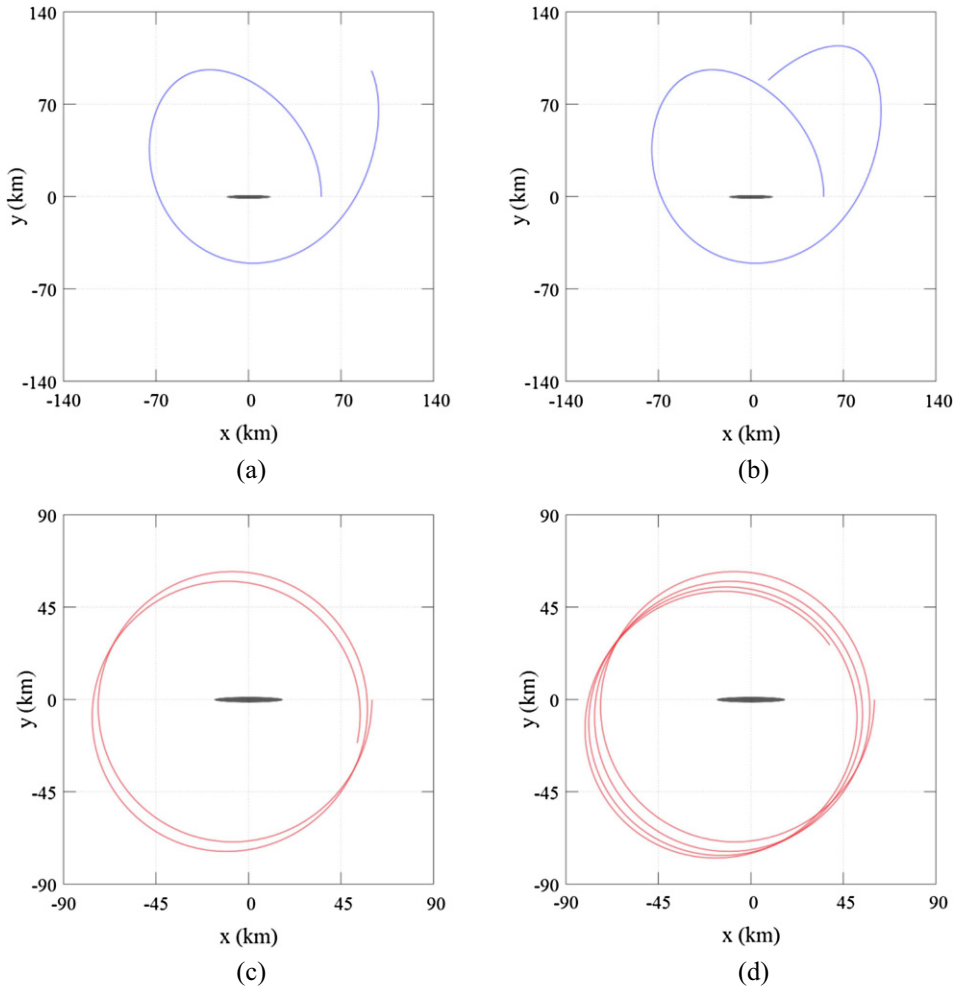
Fig. 7. Trajectories for $A/m = 0.001\,\mathrm{m}^2/\mathrm{kg}$: (a) $T = 90$ days, (b) $T = 120$ days for set 1; (c) $T = 90$ days, (d) $T = 180$ days for set 2.

Table 3. Values of distances and effects of the forces for the trajectories with $A/m = 0.001\,\mathrm{m}^2/\mathrm{kg}$, considering set 1 and set 2.

	Set 1		Set 2	
	90 days	120 days	90 days	180 days
$D_{\max}$ (km)	133.4690	137.1071	79.1862	79.1862
$D_{\min}$ (km)	50.0336	50.0336	52.1923	52.1923
D_{avg} (km)	86.7800	96.4492	66.8559	66.8559
PertAster (km/s^2)	9.51×10^{-11}	8.09×10^{-11}	1.33×10^{-10}	1.31×10^{-10}
PertSun (km/s^2)	4.02×10^{-6}	3.50×10^{-6}	4.02×10^{-6}	2.89×10^{-6}
PertSRP (km/s^2)	$3,09 \times 10^{-12}$	2.68×10^{-12}	$3,09 \times 10^{-12}$	2.21×10^{-12}
PertJ2Aster (km/s^2)	1.74×10^{-12}	1.36×10^{-12}	2.73×10^{-12}	2.77×10^{-12}
PertJ2Sun (km/s^2)	2.21×10^{-17}	1.79×10^{-17}	2.21×10^{-17}	1.31×10^{-17}
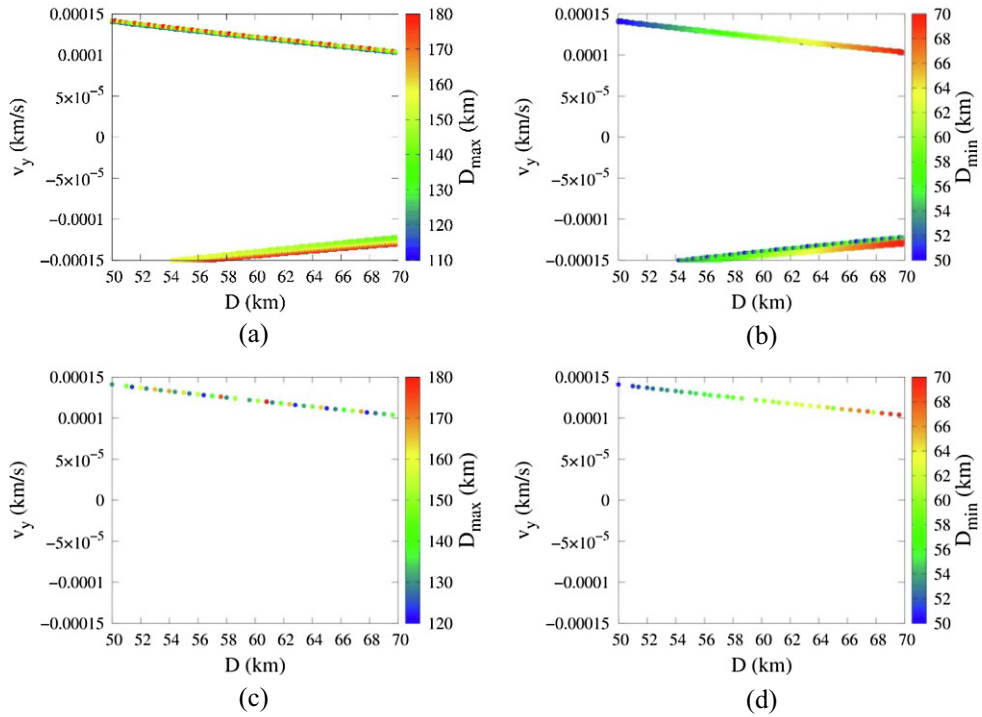
Fig. 8. Color maps for $A/m = 0.01\,\mathrm{m}^2/\mathrm{kg}$: (a) $D_{\max}$, (b) $D_{\min}$ for $T = 60$ days and (c) $D_{\max}$, (d) $D_{\min}$ for $T = 90$ days.

values of maximum (133.4690 to 137.1071 km) and average (86.7800 and 96.4492 km) distances were recorded for 90 and 120 days, respectively, as well as the lowest minimum distances (50.0336 km for both times). By analyzing the effects of the forces involved, it is observed that the Sun (PertSun) is of course the main force acting in the trajectories, being of the order of 10^{-6}, followed by the perturbation of the elongated asteroid (PertAster), which is of the order of 10^{-11} for set 1 and 10^{-10} for set 2. The effects coming from the solar radiation pressure (PertSRP) was of the order of 10^{-12} for both sets, also having values equal to 3.09×10^{-12} for both sets considering 90 days of simulation.

3.3 Study considering $A/m = 0.01\,\mathrm{m}^2/\mathrm{kg}$

In this last case, the solar radiation pressure is considered, but it is assumed a larger area-to-mass ratio for the spacecraft. It indicates the presence of a solar sail or panels. Figure 8 shows the color maps of the maximum ($D_{\max}$) and minimum ($D_{\min}$) distances as a function of the initial distance D, which varies from 50 to 70 km and the velocity v_y, that is in the range from -0.00015 to 0.00015 km/s, with the velocity v_x being fixed in zero. Figures 8a and 8b consider a time of integration of 60 days, while Figures 8c and 8d are made using a time of 90 days.

In Figure 8 the same set of initial conditions used in the two previous cases is used here to construct the color maps. In the present case, it is observed that the initial conditions that generate the trajectories having negative values of v_y, visible in Figures 9a and 9b, are not present in Figures 9c and 9d. It means that when these initial conditions are propagated for longer times, the trajectories do not

Table 4. Values of distances and effects of the forces for trajectories with $A/m = 0.01\,\mathrm{m}^2/\mathrm{kg}$ considering set 1 and set 2.

	Set 1		Set 2	
	60 days	90 days	60 days	72 days
$D_{\max}$ (km)	121.1644	121.2275	162.8198	181.4791
$D_{\min}$ (km)	65.000	59.0538	68.0000	68.0000
D_{avg} (km)	107.4641	107.6930	127.8381	128.9178
PertAster (km/s^2)	5.60×10^{-11}	5.42×10^{-11}	4.27×10^{-11}	4.17×10^{-11}
PertSun (km/s^2)	4.66×10^{-6}	4.02×10^{-6}	4.66×10^{-6}	4.40×10^{-6}
PertSRP (km/s^2)	3.58×10^{-11}	3.09×10^{-11}	3.58×10^{-11}	3.38×10^{-11}
PertJ2Aster (km/s^2)	5.32×10^{-13}	5.28×10^{-13}	3.57×10^{-13}	3.32×10^{-13}
PertJ2Sun (km/s^2)	2.78×10^{-17}	2.21×10^{-17}	2.78×10^{-17}	2.54×10^{-17}

respect at least one of the maximum and minimum distances restrictions. Through the distribution of maximum distances, shown in Figure 9a, it is observed that these conditions probably no longer respect the restriction $D_{\max} < 180\,\mathrm{km}$, because for the time of 60 days the system was already close to the limit value. Compared to previous simulations it is clear that the regions of initial conditions are even smaller for this higher value of the solar radiation pressure.

Figure 9 presents two examples of trajectories, with the two sets of initial conditions taken from Figure 8. Set 1 considers $D = 65\,\mathrm{km}$, $v_x = 0$, and $v_y = 0.000112\,\mathrm{km/s}$; while set 2 considers $D = 68\,\mathrm{km}$, $v_x = 0$, and $v_y = -0.00013\,\mathrm{km/s}$. Figure 9a and 9b show trajectories for set 1 considering the times of 60 and 90 days, respectively. Figure 9c and 9d show trajectories for set 2 considering times of integration of 60 and 72 days, respectively. The idea is to show a trajectory that "survives" up to 90 days, given by set 1, and a trajectory that does not "survive" up to 90 days, given by set 2. The rotating reference system is used, and the elongated asteroid is represented in scale at the origin of the system. It is observed that set 1 shows a trajectory that starts at $D = 65\,\mathrm{km}$ and moves counterclockwise, up to a certain point when it turns right and start to move clockwise, as visible in Figure 7a. However, Figure 7b shows that the trajectory tends to move towards the elongated asteroid, and it is likely that, in a short time, it will no longer respect the limit of $D_{\min} > 50\,\mathrm{km}$. Figure 9c shows a trajectory that starts at $D = 68\,\mathrm{km}$ and moves clockwise for a certain time, when it enters in a loop and goes counterclockwise. In Figure 9d it is observed that the trajectory continues to move away from the elongated asteroid and, in 72 days, it is already outside the limit of $D_{\max} < 180\,\mathrm{km}$.

Table 4 shows the maximum, minimum, and average distances; as well as the effects of the gravitational forces and the J_2 terms of the flattening of the Sun and the elongated asteroid for each trajectory.

Observing set 1 in Table 4, it can be seen that the maximum distance has a small increase when the time goes from 60 to 90 days, having values equal to 121.1644 and 121.2275 km, respectively. However, the minimum distance decreases from 65.000 to 59.0538 km with the increase of the simulation time. Observing set 2, in Table 4, it can be seen that the maximum distance increases from 162.8198 to 181.4791 km, considering the times of 60 and 72 days. It is also observed that the minimum distance remained equal to 68.0000 km over the simulation time.

By analyzing the effects of the forces acting in the system, it is observed that the Sun (PertSun) dominates the trajectories, as in the other cases, with a contribution in the order of 10^{-6}, followed by the perturbation of the elongated asteroid (PertAster), which is on the order of 10^{-11} for sets 1 and 2. The effects of the solar radiation pressure (PertSRP) are of the order of 10^{-11} for both sets.
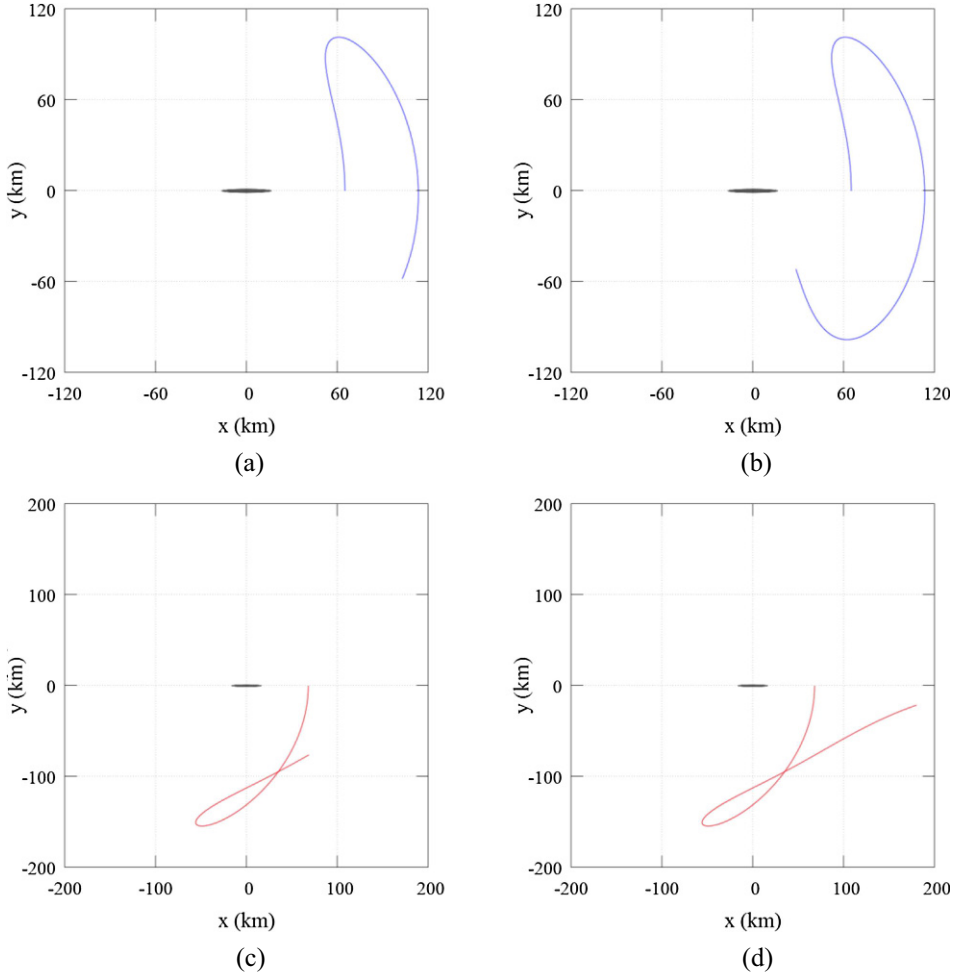
Fig. 9. Trajectories for $A/m = 0.01 \, \mathrm{m}^2/\mathrm{kg}$: (a) $T = 60$ days, (b) $T = 90$ days for set 1; (c) $T = 60$ days, (d) $T = 72$ days for set 2.

3.4 Comparing the results obtained between the three values of A/m: zero, 0.001, and 0.01 m²/kg

Some important points are now highlighted by analyzing the results for the three values of A/m, since we used the same set of initial conditions for the creation of the color maps and the time of simulation of 90 days for all the cases. Those points are listed next:

– As the value of A/m is increased, a reduction of the initial condition that generates trajectories following the distance limits $D_{\max} < 180 \, \mathrm{km}$ and $D_{\min} > 50 \, \mathrm{km}$ for the 90 days was observed. Comparing the cases with the solar radiation pressure, using values of A/m equal to 0.001 and 0.01 m²/kg, with the case without solar radiation pressure, $A/m = 0$, there was a decrease of approximately 57% and 99%, respectively.
– It was also observed that the values of initial conditions with the lowest values of initial distance D, which are the ones starting close to the elongated asteroid, are those that tend not to respect the limits of distances with the increase of A/m.

- With the increase of A/m it was also observed that the longer simulation times used to generate the color maps decreased. The highest time for $A/m = 0$ was 240 days and could have been even longer, since the trajectories "survived" without large oscillations over the time. For $A/m = 0.001\,\mathrm{m^2/kg}$ the time was 180 days, since the trajectories presented very different behaviors and stronger oscillations. For $A/m = 0.01\,\mathrm{m^2/kg}$ the longest time was equal to 90 days, presenting only a thin range of results and trajectories that do not move around the asteroid and tend to escape or collide with it.
- The Sun dominates the motion, as expected, with PertSun in the order of 10^{-6}.
- The effects of the gravity of the elongated asteroid (PertAster) vary depending on how close the spacecraft passes by the asteroid, but it is in order of magnitude from 10^{-10} to 10^{-11}.
- The order of magnitude of the effects of the solar radiation pressure (PertSRP) increased by an order of magnitude when increasing the A/m from 0.001 to $0.01\,\mathrm{m^2/kg}$, as expected, and it goes from 10^{-12} to 10^{-11}.

4 Conclusion

In this study it was possible to identify numerous sets of initial conditions that can be used to place a spacecraft in orbit around an elongated asteroid that respect lower and upper distance limits during the whole trajectory. Using color maps it was possible to identify those ranges of initial conditions. Those orbits increase the options of trajectories that can be used depending on the goal of the mission.

It was also observed that the sizes of the intervals of initial conditions change according to whether or not the solar radiation pressure is considered and the value of A/m. Those sizes decrease with A/m, which means that the solar radiation pressure strongly disturbs the orbits making them to get too close or too far from the system. Even when initial conditions are found, their durations are smaller when solar radiation pressure is acting in the system.

Another point observed, making calculations of the integrals of the accelerations involved in the problem, is that it is possible to identify the importance of each force acting in the system for each trajectory. The Sun is the dominant force, as expected, with an integral in the order of 10^{-6}, followed by the gravity of the elongated asteroid (ranging from 10^{-11} to 10^{-10}) and the solar radiation pressure (ranging from 10^{-12} to 10^{-11}). The effects of the flattening of the elongated asteroid (term J_2 of the gravity field) range from 10^{-13} to 10^{-12} and the equivalent term for the Sun is of the order of 10^{-17}.

Author contribution statement

Cavalca carried out program data adjustments, simulations and sketched text. Gomes contributed to the programming of the software and adjustments in the text. Diogo contributed to the presentation and analysis of the results. All the results and the final text were discussed by all the authors.

Publisher's Note The EPJ Publishers remain neutral with regard to jurisdictional claims in published maps and institutional affiliations.

References

1. NASA, *NSSDCA – Solar system exploration*, https://nssdc.gsfc.nasa.gov/planetary/ [Retrieved 1 May 2019]
2. M. Massironi et al., Nature **526**, 402 (2015)
3. J. Fang, J.L. Margot, M. Brozovic, M.C. Nolan, L.A.M. Benner, P.A. Taylor, Astron. J. **145**, 154 (2011)
4. F. Braga-Ribas et al., Nature **508**, 72 (2014)
5. J.L. Ortiz et al., Nature **550**, 219 (2017)
6. Z. Zhenjiang, Y. Meng, C. Hutao, C. Pingyuan, IPCSIT **53**, 135 (2012)
7. L.B.T. dos Santos, A.F.B. de Almeida Prado, D.M. Sanchez, Astrophys. Space Sci. **362**, 202 (2017)
8. ESA, *Rosetta*, http://www.esa.int/Our_Activities/Space_Science/Rosetta [Retrieved 1 May 2019]
9. S. Lowry et al., Astron. Astrophys. **548**, A12 (2012)
10. R.A.N. Araujo, O.C. Winter, A.F.B.A. Prado, Mon. Not. R. Astron. Soc. **449**, 4404 (2015)
11. R.A.N. Araujo, O.C. Winter, A.F.B.A. Prado, A. Sukhanov, Mon. Not. R. Astron. Soc. **423**, 3073 (2012)
12. B.Y.P.L. Masago, A.F.B.A. Prado, A.P.M. Chiaradia, V.M. Gomes, Adv. Space Res. **57**, 962 (2016)
13. A. Sukhanov, H. Velho, E. Macau, O.C. Winter, Cosmic Res. **48**, 443 (2010)
14. A. Sukhanov, A.F.B.A. Prado, Adv. Space Res. **50**, 1478 (2012)
15. S. Da Silva Fernandes, W.A. Golfetto, Math. Probl. Eng. **2007**, 23 (2007)
16. S. Geffroy, R. Epenoy, Acta Astronaut. **41**, 133 (1997)
17. B.N. Kiforenko, Int. Appl. Mech. **41**, 1211 (2005)
18. A.F.B.A. Prado, G. De Felipe, Adv. Space Res. **40**, 102 (2007)
19. A. Rossi, F. Marzari, P. Farinella, Earth Planets Space **51**, 1173 (1999)
20. V. Szebehely, *Theory of orbits* (Academic Press, New York, 1967)
21. D.M. Sanchez, T. Yokoyama, P.I.O. Brasil, R.R. Cordeiro, S.M.G. Winter, Math. Probl. Eng., **2009**, 15 (2009)
22. O. Montenbruck, E. Gill, *Satellite orbits* (Springer-Verlag, Berlin, Heidelberg, 2001), pp. 77–79
23. A.F.B.A. Prado, Adv. Space Res. **53**, 877 (2014)
24. D.M. Sanchez, A.F.B.A. Prado, T. Yokoyama, Adv. Space Res. **54**, 1008 (2014)
25. M.P.O. Cavalca, A.F.B.A. Prado, J.K.S. Formiga, V.M. Gomes, J. Phys.: Conf. Ser. **911**, 012008 (2017)
26. M.P.O. Cavalca, A.F.B.A. Prado, J.K.S. Formiga, V.M. Gomes, D.M. Sanchez, Rev. Mex. Astron. Astrofis. **54**, 729 (2018)
27. NASA. *Sun fact sheet*, https://nssdc.gsfc.nasa.gov/planetary/factsheet/sunfact.html [Retrieved 1 May 2019]
28. G. Obrecht, Exploration of optimal orbits in the strongly perturbed environment of the 2001SN$_{263}$ triple asteroid system, Master thesis Report, Aerospace Engineering, Delft University of Technology, Holand, 2016, p. 9
29. A.F.B.A. Prado, Math. Probl. Eng. **2013**, 1 (2013)
30. D.M. Sanchez, A.F.B.A. Prado, T. Yokoyama, Adv. Space Res. **54**, 1008 (2014)
31. D.M. Sanchez, A.F.B.A. Prado, On the Use of Mean Motion Resonances to Explore the Haumea System, in *Proceedings of the AAS/AIAA Astro. Spec. Conf., Stevenson, WA* (2017), Vol. 162, pp. 1507–1524